Archives of Civil and Mechanical Engineering (2021) 21:29
https://doi.org/10.1007/s43452-021-00185-8

REVIEW ARTICLE

Recent advances in the kinetics of normal/abnormal grain growth: a review

Fateme Najafkhani[1] · Sara Kheiri[1,2] · Bita Pourbahari[2] · Hamed Mirzadeh[1]

Received: 21 September 2020 / Revised: 16 January 2021 / Accepted: 23 January 2021 / Published online: 14 February 2021

Abstract
Recent progress in the kinetics of grain coarsening and abnormal grain growth (AGG) is presented in this overview article. The factors affecting the kinetics of grain growth is reviewed with the emphasis on the recent findings on the solute drag and Zener pinning effects as well as the special case of duplex alloys, where the latter is discussed for the behavior of dual-phase steels during intercritical annealing. The common isothermal kinetics models for grain growth are listed, which is followed by the critical discussion on the simplifications and the commonly used methods for the determination of grain growth exponent (n) and activation energy (Q). The obtained values of n and Q for several classes of important engineering alloys such as microalloyed steels, stainless steels, magnesium alloys, aluminum alloys, titanium alloys, and high-entropy alloys are summarized with the discussion on the obtained values of kinetics parameters and their deviation from the theoretical expectations. Finally, the factors leading to AGG (such as the coarsening and dissolution of pinning particles and the crystallographic texture), the proposed mechanisms (such as the solid-state wetting and the grain boundary faceting/defaceting phenomena), and the kinetics of AGG (based on the empirical power law and the similarity of AGG to primary recrystallization in the form of secondary recrystallization) are reviewed. This overview can shed light on the understanding of grain growth and its effects.

Keywords Grain growth kinetics · Abnormal grain growth · Inhibition of grain growth · Grain boundary migration · Solute drag effect · Particle pinning

1 Introduction

As an interesting and important field of materials science and engineering, grain growth (and its kinetics) has been an important subject since early publications [1]. Moreover, this subject has received considerable attention in recent years [2]. The surface energy of the grain boundaries is the driving force for grain growth [3]. Though often called grain growth, the term grain coarsening is also widely used.

There are two forms of grain growth: normal and abnormal. In the former, the central mechanism is the loss of the smallest grains, while maintaining a nearly constant grain size distribution [4]. On the other hand, during abnormal grain growth (AGG), some grains significantly grow by consuming the smaller grains, and hence, it is also known as secondary recrystallization. It is also referred to as exaggerated grain growth or discontinuous grain growth. In this way, a bimodal distribution is achieved for the grain size. However, the normal grain growth mode might be subsequently resumed after impingement of the large grains [5]. The normal/abnormal/normal transition sequence can be clearly seen for an austenitic stainless steel in Fig. 1a [6]. For a friction stir welded low carbon steel plate, the base metal (BM) showed a continuous grain growth while the grain growth in the fine-grained stir zone (SZ) showed three stages as shown in Fig. 1b: (I) The early annealing period with slow grain growth rate, (II) the development of AGG, and (III) the normal grain growth after completion of the AGG [7].

Interestingly, four stages of grain growth as a function of annealing temperature have been observed (Fig. 1c). The highest temperature fourth stage of growth has the lowest activation energy, which is similar to that of grain boundary

✉ Hamed Mirzadeh
hmirzadeh@ut.ac.ir

[1] School of Metallurgy and Materials Engineering, College of Engineering, University of Tehran, P.O. Box 11155-4563, Tehran, Iran

[2] Department of Materials Science and Engineering, McMaster University, Hamilton, ON L8S 4L8, Canada

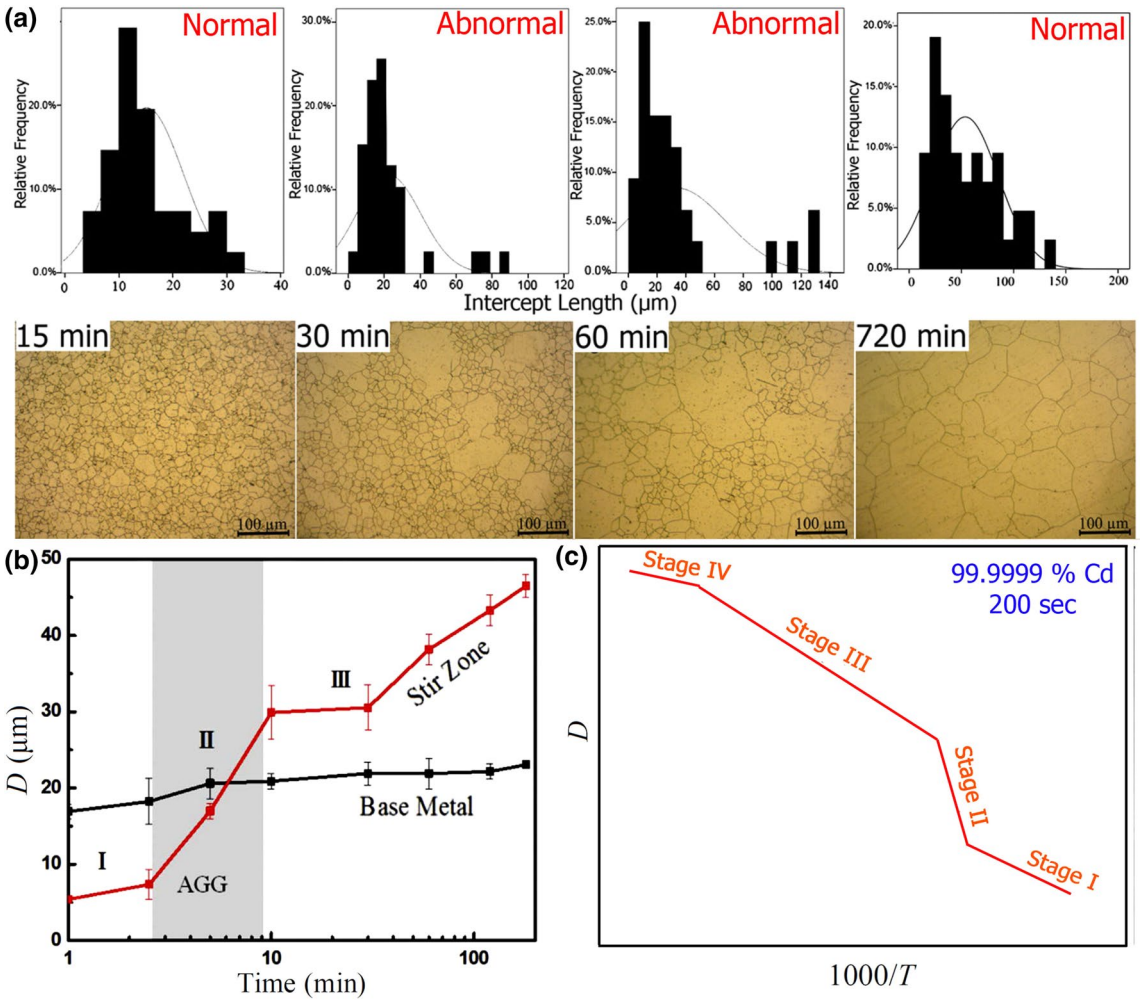

Fig. 1 **a** Optical micrographs and the corresponding grain-size distribution histograms obtained upon annealing of AISI 304L stainless steel at 900 °C [6], **b** the relationship between the average grain size and the annealing time for friction stir welded SPCC steel plates [7], and **c** schematic representation of grain growth stages for cadmium (redrawn based on [8])

self-diffusion. The first and third stages of growth have activation energies which are similar to that of volume self-diffusion. The second stage of grain growth involves AGG. In general, activation energies for grain growth are quoted as being consistent with values for volume diffusion or grain boundary diffusion, which is in general about half that for volume diffusion [8].

The computer simulation of grain growth [9], grain growth in nanostructured materials [10], understanding the mechanisms of abnormal grain growth [11], grain growth in thin films [2], grain growth during welding [12], grain growth of heat-resistant superalloys [13], and grain growth of newly developed high-entropy alloys (HEAs) [14] are among the hot topics of recent studies. However, based on its importance, the kinetics of grain growth has remained one of the most widely investigated topics. For the normal grain growth, the observed grain growth kinetics can be represented by one of the following formulae:

$$D^n - D_0^n = Kt \tag{1}$$

$$D - D_0 = Kt^{1/n} \tag{2}$$

where D, D_0, t, n, and $1/n$ are respectively the grain size, initial grain size, time, grain growth exponent, and time exponent for grain growth. Moreover, K is a temperature-dependent constant as expressed by the following equation:

$$K = K_0 \exp(-Q/RT) \tag{3}$$

where T is the temperature, K_0 is a constant, Q is the grain growth activation energy, and R is the gas constant. Based on the experimental data, the values of n and Q can be determined, which are the basis for the kinetics analysis and growth mechanisms.

Several methods/simplifications are usually applied for calculation of these kinetics parameters but their outcomes

might be inconsistent [15], and hence, the inferred mechanisms of grain growth might be different [16]. Accordingly, this subject needs to be critically discussed. Moreover, the obtained values of n and Q for different alloys should be summarized to infer useful trends from the materials science point of view, especially for recently introduced materials such as HEAs.

Moreover, while Eqs. 1–3 are the most widely used kinetics formula, other models have been developed and successfully applied to the grain growth kinetics of different engineering alloys, which should be discussed.

The kinetics of AGG kinetics [17] is similar to primary recrystallization and might be modeled by sigmoidal functions, which needs more attention. On the other hand, new evidences for the mechanisms of AGG in stainless steels [6], dual-phase (DP) steels [18], rare-earth containing magnesium alloys [19], and other alloys have been recently reported, which should be reviewed. Moreover, there is a recent progress on the understanding of grain growth based on the solute drag effect (e.g. in single-phase austenitic stainless steels and HEAs) and in the presence of second phases (e.g. during intercritical annealing of the ferritic-martensitic dual-phase steels) [16].

In response, the present work is dedicated to providing an overview of the aforementioned topics. Firstly, the factors affecting the kinetics of grain growth with the emphasis on the recent progress in this field will be introduced. Then, the kinetics models proposed for grain growth will be listed. Afterwards, the used methods and common simplifications of the general grain growth formula (Eq. 1) will be critically discussed. The obtained values of kinetics parameters (n and Q) for several classes of important engineering alloys will be also summarized. Moreover, these values will be correlated to the controlling atomic mechanisms and an updated summary of the sources of deviation from the theoretical values will be presented. Finally, the new results on the mechanisms of AGG and its kinetics will be reviewed. It should be noted that some of the important topics such as the mobility of grain boundaries and computer modeling have been comprehensively reviewed [20], and they will not be considered in this work.

2 Factors affecting grain growth kinetics

In this section, recent progress in the understanding of the influencing factors on grain growth will be treated, including temperature, pinning, and texture. However, other important factors such as specimen size, initial structure, and free-surface effect will not be discussed [3].

2.1 Temperature

Grain boundary mobility exponentially depends on the temperature and in turn affects grain growth kinetics [21]. Another indirect effect of temperature is through coarsening/dissolution of second phase particles pinning grain boundaries [22]. The latter effect can be seen in Fig. 2a, where the dissolution of β-$Mg_{17}Al_{12}$ phase at elevated temperatures in AZ61 magnesium alloy takes part in the rapid coarsening of grains; whereas in the case of Mg-4.8Gd-1.2Al-1Zn alloy (Fig. 2b), the presence of fine and widely distributed particles of the thermally stable $(Mg,Al)_3Gd$ phase significantly inhibited the growth of grains [19].

Moreover, the inhibition effect of segregating solute atoms to the grain boundaries is temperature dependent [23]. In fact, the concentration of the solute atoms in the boundaries (c) decreases by increasing temperature based on $c \propto \exp(U/RT)$. A point might be reached where the segregated impurities (e.g. Mo in stainless steels [15]) no longer able to keep up with the boundaries and the boundaries can move freely [20]. The importance of this effect has been shown in Fig. 2c: during annealing of a cold rolled AISI 316 stainless steel, after completion of reversion of strain-induced martensite to austenite, the primary recrystallization of the retained austenite and grain growth are severely inhibited at an annealing temperature of 750 °C but these processes show fast kinetics at 1000 °C [24]. Similar effects have been reported for AISI 304L stainless steel [25].

As a thermally-activated process, grain growth needs elevated temperatures for diffusion processes [3]. Therefore, based on activation energy plots obtained from the kinetics analysis, the grain growth temperature can be deduced as shown in Fig. 3 for the AISI 304 and 316 stainless steels, where the grain coarsening temperature of the latter is ~ 140 °C higher than that of the former due to the inhibition effect of 2 wt% solute Mo in the latter [15]. A similar effect has been reported for the effect of AlN on the austenite grain growth in fine-grained Al-killed steels, which exhibits almost no grain growth at low austenitizing temperatures, but a discontinuous increase in grain size occurs at a temperature known as the grain-coarsening temperature. This behavior is consistent with secondary recrystallization, which is caused by the precipitation of fine AlN particles and their eventual dissolution at the grain-coarsening temperature. In contrast, austenite grain size increases continuously with increasing temperature in the coarse-grained steel (deoxidized with silicon), even at low temperatures [26]. In fact, Al can help to control grain growth at medium temperatures, but its addition to Ti steels can promote abnormal grain growth [27].

Grain growth at high temperatures might be also important during the hot deformation of engineering alloys. For instance, an instability region was observed at high

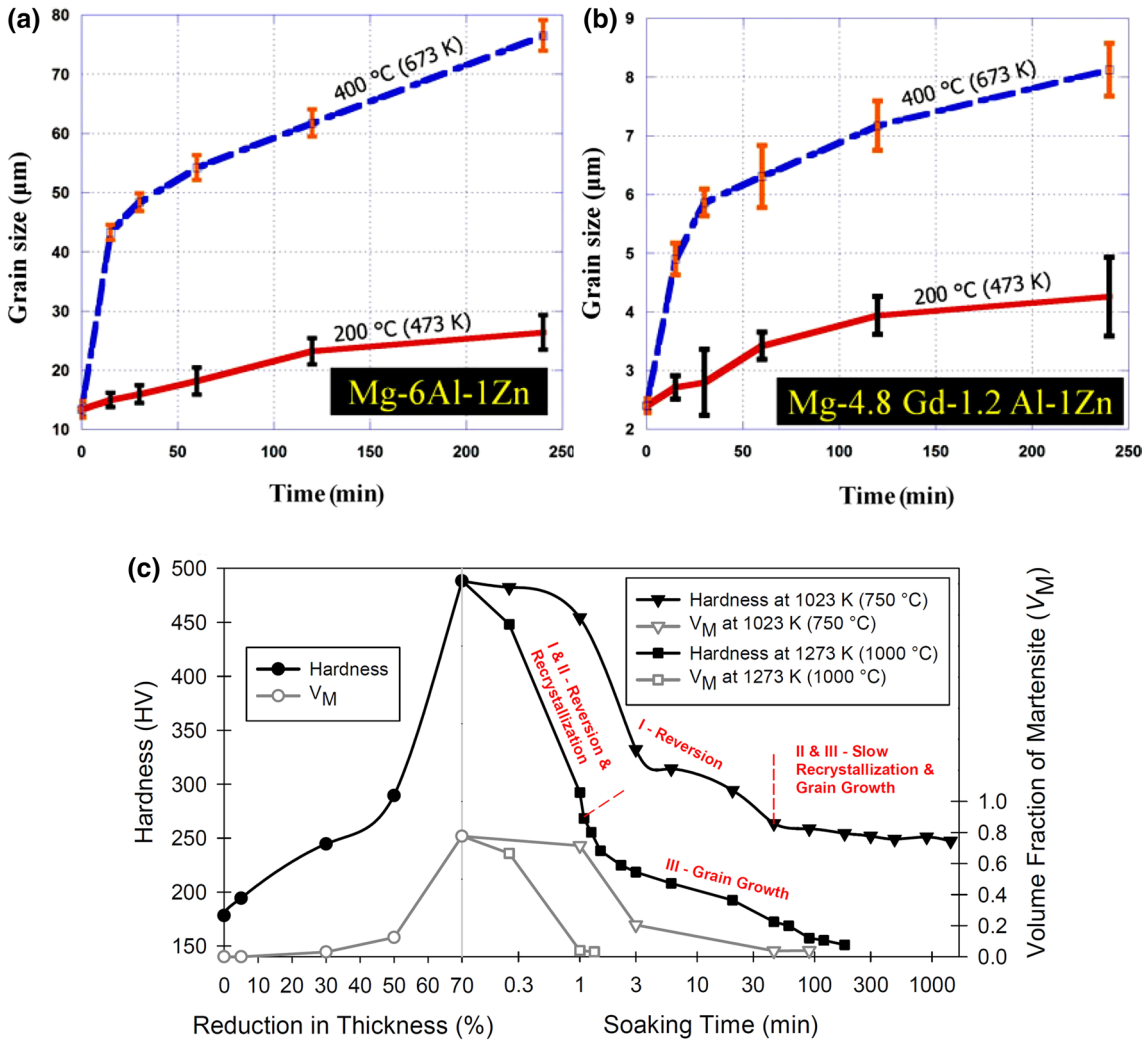

Fig. 2 **a**, **b** Grain growth curves of two Mg alloys [19] and **c** Hardness and amount of strain-induced martensite during cold rolling and subsequent annealing of AISI 316 stainless steel [24]

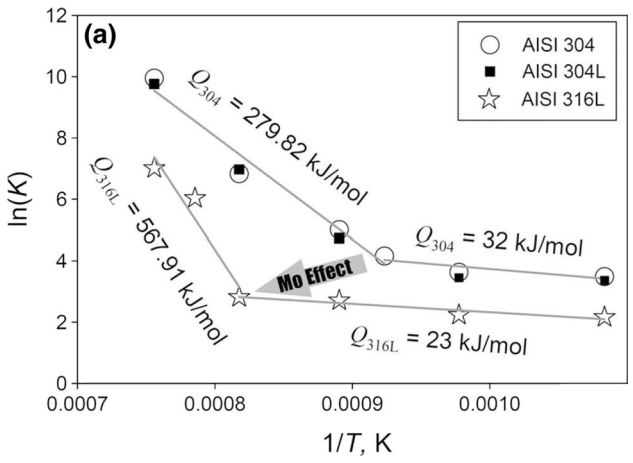

Fig. 3 Activation energy plots to deduce the effect of C and Mo as alloying elements on the high-temperature grain growth behavior of commercial austenitic stainless steels [15]

temperature and low strain rates for Mg-Gd binary alloys, which was ascribed to grain growth or even partial melting due to high exposure time at high temperatures [28]. Moreover, for a nickel-based superalloy, the increase in deformation time under the relatively low strain rates promoted the growth of dynamic recrystallization (DRX) grains [29]. Even, AGG has been recognized as a critical issue during hot deformation of FSP-processed Al alloys [30].

2.2 Pinning effects

Primarily the pinning is caused by solute drag, Zener pinning of finely dispersed particles, pinning by the second phase in duplex alloys, and orientation pinning. Whatever might be source, extent of pinning often gives rise to different mobilities of different types of grain boundaries [5]. It should be also noted that holes or pores can have the same

effect on grain-boundary motion as second-phase particles [31], which is known as the pore drag effect and it is noticed in powder metallurgy parts, especially in nanocrystalline materials [32].

2.2.1 Solute drag

Regarding the solute drag effect, the solute atoms segregate to grain boundaries, where the pinning effect becomes considerable at relatively low temperatures. The grain boundaries have to drag the solute atoms to move together. Thus, the grain boundary movement is inhibited by the solute drag effect. With the temperature increasing, the velocity of the grain boundary rises, and the cloud of segregation solute atoms gradually disappears. Once the temperature reaches a critical value, the driving force of grain boundary movement is no longer balanced with the tension stress of the solute cloud, so the grain boundaries gradually cast off the solute segregation. As a consequence, the diffusion rate of solute atoms in solution can keep up with the grain boundary movement, and the solute drag effect is no longer obvious in the high-temperature region. This effect has been shown in low carbon Nb microalloyed steels [33].

A striking solute drag effect has been observed for Mo segregation in austenitic stainless steels as shown in Fig. 4, where it can be seen that the Mo addition severely retarded the grain growth. This figure also shows the effect of interstitial carbon atoms on grain growth, where it can be seen that the addition of C promoted the coarsening of grains [15]. While a similar effect for C has been acknowledged in microalloyed [34] and low alloy [35] steels, this effect seems to be marginal. The value of the activation energy for grain growth (assumed to be the activation energy for the diffusion of Fe in austenite) depends on the chemical composition of the steel. Interstitial elements, such as carbon, decrease the activation energy and increase the austenite grain size [35].

For HEAs, there are abundant solutes in the random solid-solution state, a mechanism not found in conventional alloys based on one major element. As a result, the solute-drag effect is significant in the whole-solute matrix of HEAs, as compared with the conventional solid-solution alloy. This trend is related to the energy incurred during different sizes of abundant solutes along grain boundaries in-situ adjusting their relative positions to form the low-energy configuration of grain boundaries during boundary migration [14].

2.2.2 Zener pinning

Grain growth might be ceased by particle pinning and a limiting grain size might be reached [3]. For Zener pinning, the effect of particles with radius of r (diameter of $d=2r$) and volume fraction of f on the limiting grain size (D_l) is described by the Smith–Zener-type relation [35]:

$$D_l \propto r/f \tag{4}$$

In a microstructure comprising of grains with average radius of $\overline{R}$, Fig. 5 has been developed to show the effect of particles on grain growth based on the plot of $\overline{R}$ versus dispersion level (f/d) [36], where the appearance of the AGG regime is an important issue [37] and it will be treated later.

The coarsening of pinning particles at elevated temperatures from r_0 to r for the time t (Ostwald ripening) should be also considered, where based on the diffusivity D, its kinetics is described by the Lifshitz–Wagner-type relation [3]:

$$r^3 - r_0^3 \propto Dt \tag{5}$$

Accordingly, besides the strong effect of r and f on the particle pinning effect, the resistance to particle coarsening

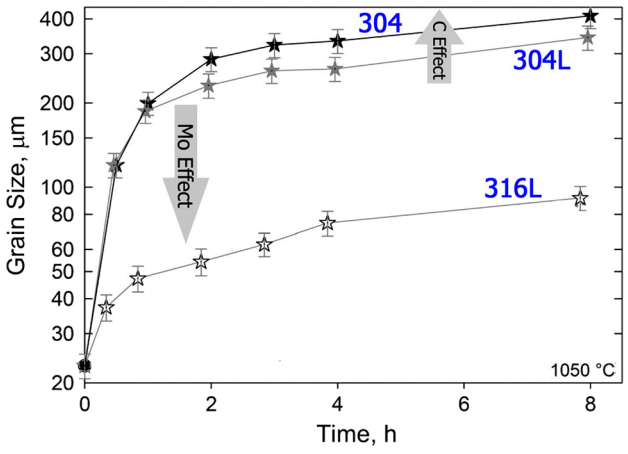

Fig. 4 Grain size versus annealing time for austenitic stainless steels [15]

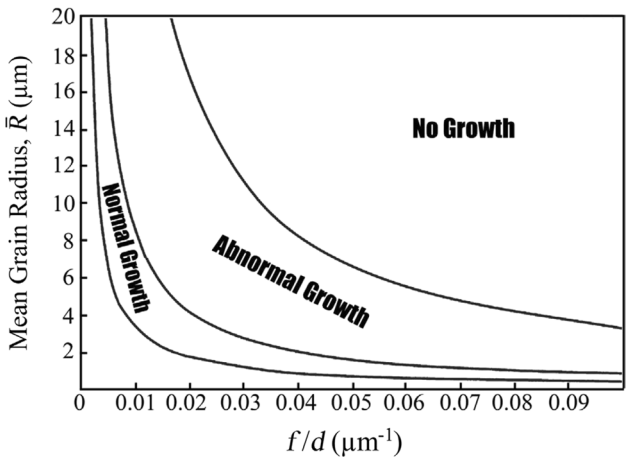

Fig. 5 The various growth regimes for an ideal grain assembly [36]

is an important factor [38]. In microalloyed steels, the addition of Ti, Nb, and V has been noted for austenite grain size control via precipitation of carbonitrides [39]. The austenite grain size is shown to result from the competition between a driving pressure for grain growth and a pinning pressure induced by precipitates that evolves during heat treatments [40].

In the context of superplasticity, the pseudo single-phase alloys are processed to develop a dispersion of fine precipitates so that on recrystallization the alloy will have a small grain size due to the pinning action of the dispersoids on the grain boundaries (i.e. Zener pinning). Moreover, fine precipitates will also inhibit dynamic grain growth during superplastic forming, which in Al alloys is a particularly important consideration since superplastic deformation is usually carried out at relatively high temperatures [41]. It has been shown that superplasticity can be achieved when the average grain size (D) is finer than the projected subgrain size (λ, which inversely depends on the applied stress). For $D < \lambda$, the stress concentration at the triple junction during grain boundary sliding (GBS) can be effectively revealed/accommodated via dislocation glide in the adjacent blocking grain. These intragranular dislocations pile-up at the opposing grain boundary and are subsequently removed by climb into the boundary to anable further GBS. Accordingly, the grains retain essentially their original shape and they become displaced with respect to each other so that there is a net increase in the number of grains measured along the tensile axis (Rachinger sliding), and in this way, a very high elongation to failure can be achieved by the GBS process. In the case of $D > \lambda$, the subgrains are effective obstacles for these processes and impair the superplastic properties. This effect is shown in Fig. 6 and it can be deduced that grain growth during superplastic forming might result in the situation where $D > \lambda$. Therefore, the inhibition of grain growth is of utmost importance. Typically, a grain size finer than 10 μm is required for superplasticity [42].

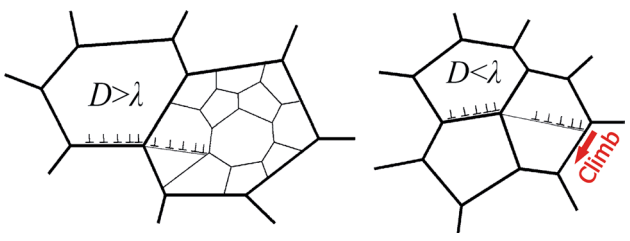

Fig. 6 Schematic illustrations of a unified model for grain boundary sliding in conventional creep when $D > \lambda$ and superplasticity when $D < \lambda$ [42]

2.2.3 Duplex alloys

In duplex alloys (such as duplex stainless steels, α/β titanium alloys [43], superalloys [44] via controlled precipitation [45], and DP steels [46]), grain growth is limited by having a microstructure consisting of significant proportions of two, or more, chemically and structurally different phases [41]. The microduplex alloys are thermomechanically processed to develop a fine grain/phase size, which is applicable in superplastic forming to inhibit grain growth at elevated temperatures.

Recently, grain growth of ferritic-martensitic DP steels has received attention, which stems from the need for intercritical annealing treatment to develop the required microstructure in these steels [16]. The intercritical annealing time should be long enough to obtain the equilibrium amount of austenite (or martensite after water quenching from the intercritical annealing temperature) but longer holding times can lead to grain growth [16], and in some cases, abnormal grain growth [37]. The coexistence of austenite at the intercritical annealing temperature can retard the grain growth of ferrite. The grain growth curves during the intercritical annealing of DP steel are shown in Fig. 7a.

It can be seen that at each temperature, by increasing the holding time, the grain size increased. However, by increasing the annealing temperature the grain growth rate firstly increased, but at higher temperatures, the kinetics in contrast became slower. Indeed, by increasing the annealing temperature, a faster grain growth rate is expected. However, at the same time, the amount of austenite as the second phase in DP steel also increases with the consequent grain boundary pinning [16]. These two factors compete, and hence, after the formation of a certain amount of martensite, it is possible that the pinning effect counteracts the temperature effect. The balance of these two competing processes results in the appearance of an intermediate temperature that leads to the highest grain growth rate. Since this retardation effect with respect to the grain boundary migration is important during grain growth, the AGG might happen at long annealing times [37], which might significantly deteriorate the mechanical properties of the material, as shown in Fig. 7b for DP steel [16]. A similar deteriorative effect of AGG has been also confirmed for AZ21 Mg alloy [47].

2.3 Crystallographic texture

Pronounced texture, resulting from the initial thermomechanical processing treatment, has a marked influence on grain growth. Strong texture components might lead to the inhibition of grain growth because grains of the preferred orientation tend to be separated by boundaries of the low angle type, which are known to have low mobility. However, grains in the system which do not have this preferred

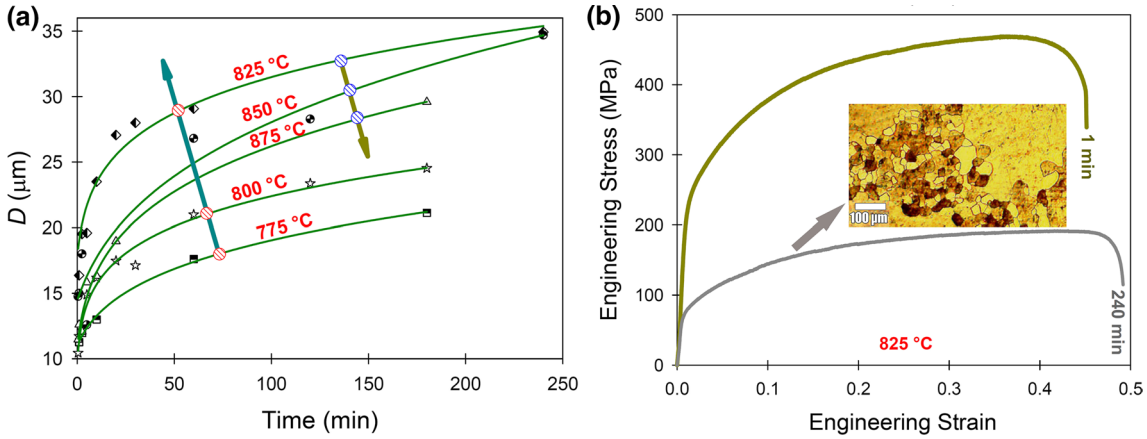

Fig. 7 **a** Grain growth curves and **b** Effect of abnormal grain growth on the engineering stress–strain curve of a 0.035C–0.27Mn–0.035Si DP steel [16]

orientation may then be favored as sites for AGG [48]. As an example, for Ti–6Al–4 V alloy [49], it was shown that a relatively strong initial texture resulted in a slow initial grain growth, but much quicker growth was achieved after a reduction in the sharpness of the texture at long annealing times. Accordingly, materials with different initial textures might exhibit noticeably different grain growth kinetics during isothermal annealing. The higher the temperature, the shorter is the exposure time necessary for fast growth to start [49].

Recently, the results of the grain growth, coupled with texture studies, have been used to infer the observed strength-ductility trends in Mg alloys [50]. Using an extruded Mg–Gd–Al–Zn magnesium alloy, it is found that by decreasing the extrusion temperature with the resulting grain refinement, both strength and ductility enhance. The enhanced strength was related to the grain refinement at lower extrusion temperatures and the enhanced ductility was related to the weakening of basal texture by Gd. However, grain growth annealing with the resulting coarsening of grains was used to elaborate these effects. The average grain size versus time during annealing at 500 °C is shown in Fig. 8a. It can be seen that grain size increases by increasing soaking time in the form of parabolic kinetics. In addition to the as-received extruded sample, the sample subjected to the soaking time of 4 h with a grain size of ~ 15 μm was tensile tested and the results are shown in Fig. 8b. It can be seen that by increasing the grain size from ~ 3 to ~ 15 μm, the tensile strength decreased and the total elongation increased. The corresponding pole figures are shown in Fig. 8c. It can be seen that the basal texture and its intensity have remained intact. Therefore, the usual strength-ductility trend was observed, in which the strength decreases but the ductility enhances via increasing the average grain size [50].

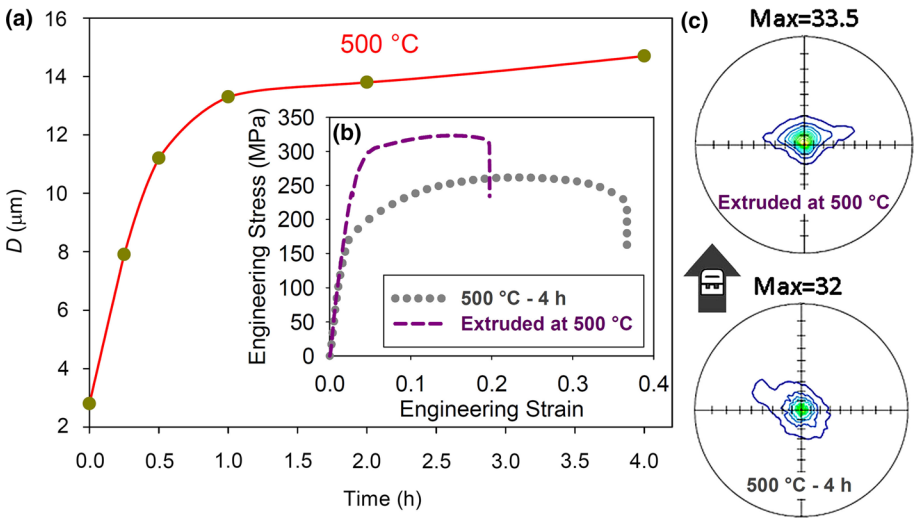

Fig. 8 **a** Grain growth curve, **b** tensile curves before and after grain growth, and **c** (0002) pole figures before and after grain growth of Mg–4.8Gd–1.2Al–1Zn magnesium alloy [50]

3 Modeling the kinetics of grain growth

3.1 Common isothermal kinetics models

Several models have been proposed for the kinetics of grain growth, where some famous ones will be presented. The simple model of Beck et al. [51] for isothermal grain growth can be expressed as $D = Kt^{1/n}$, which is similar to Eq. 2 but the effect of D_0 has not been considered. Moreover, the parameters n and K are considered to be temperature-dependent. For instance, it has been reported that the value of $1/n$ increases from 0.056 to 0.32 by increasing temperature from 350 to 600 °C for high purity Al. Therefore, the values of n decrease from ~ 18 to ~ 3. By algebraic operations, the equation of $\log(\mathrm{d}D/\mathrm{d}t) = \log(1/n) + n\log(K) + (1-n)\log(D)$ can be obtained, which leads to a straight line for each temperature in the plot of $\log(\mathrm{d}D/\mathrm{d}t)$ versus $\log(D)$ and the slope of the line is $1 - n$. However, slight initial deviations from the $D = Kt^{1/n}$ relationship are usually observed at low temperatures [51]. This might be related to the neglecting of D_0, which is important at lower temperatures since D might not be effectively higher than D_0.

The model of Burke and Turnbull [52] considers D_0 based on $D^2 - D_0^2 = (K\sigma V)t$. In this equation, σ is the surface energy of the boundary and V is the gram atomic volume. It can be seen that this model is similar to Eq. 1 but the grain growth exponent n has been fixed at 2 [51]. However, for many more alloys, the experimental data cannot be fitted by $n = 2$, and a higher value is expected. The grain growth exponent n is dependent on the temperature, material, and grain boundary pinning factors [3].

Sellars and Whiteman [53] used the equation of $D^n - D_0^n = At\exp(-Q/RT)$, which can be obtained by combining Eqs. 1 and 3. The experimental data gave a value of $n = 10$ for the grain growth of C-Mn steels after recrystallization. The large value of 10 was found to be reasonable for short times, but it decreases towards the expected value at longer times [53].

Nishizawa [54] proposed the grain growth equation of $D^n - D_0^n = (\sigma V D_{gb}/RT\delta)t$, where δ is the grain boundary thickness. It can be seen that the grain boundary self-diffusion activation energy has been used [55]. Therefore, this model is based on Eq. 1 but $K = \sigma V D_{gb}/RT\delta$ has been used instead of K formula in Eq. 3.

Raghunathan and Sheppard [56] used the equation of $D = D_0 + At^{1/n}\exp(-Q/RT)$ for grain growth following recrystallization in Al–Mg alloys. This equation can be determined by combining Eq. 2 and 3. Anelli [57] also used a similar model for C-Mn steels by neglecting D_0: $D = At^{1/n}\exp(-Q/RT)$.

Du et al. [58] argued that in the Sellars–Whiteman model [53], the holding time exponent is ignored, while in the model proposed by Anelli [57], the initial grain size is neglected. Therefore, they combined these models and proposed the equation of $D^n = D_0^n + At^m\exp(-Q/RT)$, where both grain growth exponent (n) and time exponent (m) have been considered. However, n, m, A, and Q can not be determined by linear regression [58].

It can be seen that all of the introduced models in this section have been derived from the classical Beck's model. These models can be successfully applied to predict the kinetics of grain growth. Among to the introduced models, the model described by Eqs. 1 and 3 is the most widely used one. In this model, n and Q are important parameters, which can be used to infer the mechanism of grain growth and obtaining the experimental grain growth formula. There are several methods and assumptions for this purpose, which will be discussed in the next section.

3.2 Determining *n* and *Q*

Based on Eq. 1 ($D^n - D_0^n = Kt$), the value of n can be determined at a constant temperature. When D_0 is very small compared to D, it can be ignored [59]. Then, based on $D^n = Kt$, the relationship of $\ln t = n\ln D - \ln K$ is obtained. Accordingly, at a given temperature, the slope and the intercept of the plot of $\ln t$ versus $\ln D$ can be used to obtain the values of n and $-\ln K$, respectively. This is shown for an AISI 304 stainless steel in Fig. 9a. It can be seen that the values of n decrease with an increasing temperature towards the ideal value of 2 [3]. In Fig. 9a, the results for AISI 304L stainless steel at 923 K is also shown, which reports a much lower n value (~ 7) compared to n value of ~ 24 for AISI 304 stainless steel at this temperature. This can be explained by the fact that the growth of AISI 304 is retarded by the precipitation of carbides on grain boundaries while these carbides are not present in the low carbon 304L variant [15].

Sometimes the value of D_0 in $D^n - D_0^n = Kt$ cannot be ignored. In these cases, the nonlinear regression can be used for obtaining n and K [60]. An example is shown in Fig. 9b for DP steel [16]. In fact, grain growth at the intercritical annealing temperature is not very rapid, and hence, D_0 should be considered. The resultant n values based on the consideration and neglecting of D_0 were obtained, and it was found that at high temperatures, the value of n approaches to ~ 4 and ~ 5, based on the consideration and neglecting of D_0, respectively [16]. It has been revealed that grain growth in a single-phase steel is controlled by bulk diffusion, giving $n = 2$, while n for dual-phase steels is considered to be 3 or 4 [61]. Therefore, it can be deduced that the consideration of D_0 is important in this case. In should be noted that by consideration of Eqs. 2 and 3, these problems can be avoided due to the presence of time exponent instead of grain size exponent [62].

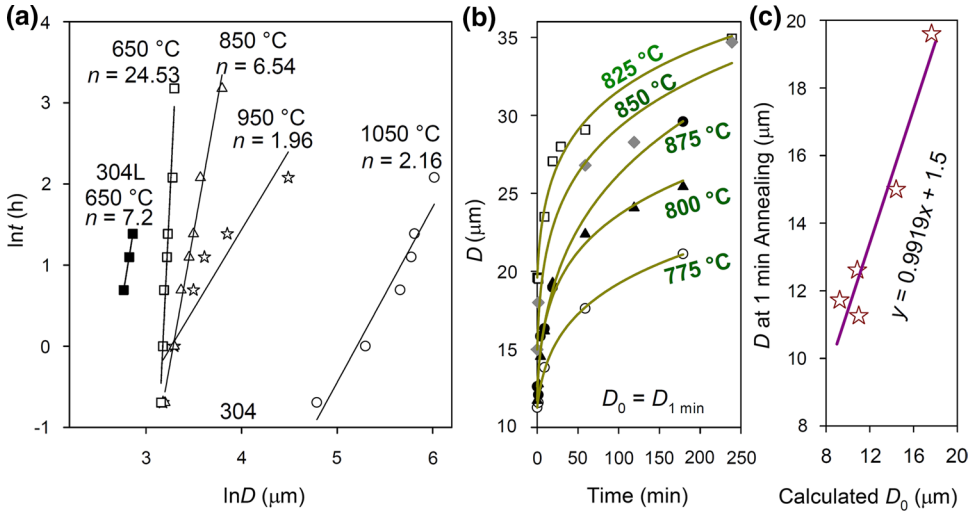

Fig. 9 **a** Obtaining n for grain growth of AISI 304 stainless steel, where for obtaining n, D_0 was temporarily neglected because both D and D_0 have been raised to the power of n [15], **b** effects of annealing temperature and holding time on the grain size of a 0.035C–0.27Mn–0.035Si DP steel by consideration of the grain size at 1 min as the initial grain size [16], **c** the obtained grain size at 1 min annealing versus the calculated initial grain size for a 0.035C–0.27Mn–0.035Si DP steel [16]

In some cases, the initial grain size cannot be determined. For instance, when a cold-rolled martensite in low carbon steels is heated to the intercritical annealing temperature, the formation of the initial ferrite–austenite mixture needs some time. In these cases, in addition to n and k, D_0 can be also considered as a fitting parameter. This is shown in Fig. 9c, where the obtained average ferrite grain size after 1 min annealing is compared to the calculated D_0 by nonlinear regression [16].

By taking the natural logarithm from Eq. 3 of the form of $K = K_0 \exp(-Q/RT)$, the equation of $\ln(K) = \ln(K_0) + (-Q/R)(1/T)$ is determined. Accordingly, the slope of the plot of ln$K$ versus $1/T$ can be used to obtain the values of $-Q$/R. An example is shown in Fig. 3. Therefore, for obtaining Q, appropriate values of K are required. As discussed above, the consideration and neglecting of D_0 results in different n values, and hence, different K values. Moreover, the values of K not only change with temperature based on $K = K_0 \exp(-Q/RT)$, but also change as a result of dependency of n on temperature and its effect on the value of K based on $D^n - D_0^n = Kt$. While the dependency of n on temperature has been observed, usually no meaningful activation energy can be obtained for the grain growth process when n varies with temperature due to its effects on the obtained K values [16]. Therefore, consideration of a predefined fixed n value is also common, where the most widely used one is the ideal value of 2 [63]. Moreover, the average n value obtained from different temperatures has been also used [16]. As a result, by fixing n, the values of K can be recalculated, and then the values of Q can be determined, where the applicability of this technique has been clearly shown [16].

By consideration of a fixed n value, it is possible to directly obtain Q without calculation of K. For instance, by taking logarithm from $D^2 - D_0^2 = K_0 \exp(-Q/RT)t$, the equation of $\log\{(D^2 - D_0^2)/t\} = \log(K_0) + (-Q/2.3R)(1/T)$ is obtained. Therefore, the slope of the plot of $\log\{(D^2 - D_0^2)/t\}$ versus $1/T$ can be used for obtaining $-Q$/2.3R [31].

By consideration of different stages of grain growth (Fig. 1c), in the third and fourth stage of grain growth, the equation of $D^2 - D_0^2 = K(t - t_0)$ has been used, where t_0 is the time at which the stages are started. It has been also argued that the multistage growth behavior is probably responsible for n being measured as less than the theoretical value of 2 in many investigations [64].

3.3 Summarizing the values of *n* and *Q*

Studying the kinetics of grain growth in commercial steels has received considerable attention [65], which is preliminary related to the dependency of mechanical properties on grain size. The obtained values of n and Q for microalloyed, low carbon, and low alloy steels are summarized in Table 1. It can be seen that a wide range of values have been determined. However, it can be inferred that at high temperatures, n is situated between 2 and 3, indicating that second phase particles in the grain provide a drag force to inhibit the growth of austenite grains [66]. Moreover, the Q values near grain boundary diffusion in austenite (143 kJ/mol) and lattice diffusion in austenite (270 kJ/mol) [63] are common. For a microalloyed steel, at low temperatures, n between 6 and 8 with an activation energy of 121 kJ/mol was obtained, that indicates inhibition of grain growth controlled by the diffusion of C or N into the austenitic phase to produce an Ostwald ripening process. However, at high temperatures, the ideal kinetic exponent of 2 was obtained, and as a result, the activation energy decreased to a mean value of 88 kJ/mol [62].

Grain growth kinetics has been studied for stainless steels [74], where the obtained parameters of the empirical power law model are summarized in Table 2. For the alloys without

Table 1 Reported values of n and Q for microalloyed, low carbon, and low alloy steels

Material	Microallying elements (wt%)	Temperature (°C)	n	Q (kJ/mol)	References
LZ50 steel	0.02 V	950–1200	2.82	336.48	[58]
hot rolled steel	–	900–1250	12.66–3.14	2943–157	[59]
GCr15 steel	–	950–1150	2.77	458	[66]
Nb-V steel	0.026 V–0.0135 Nb	1050–1150 1200–1250	8–6 2	121 88	[62]
Low alloy TRIP steel	–	1150	2	270	[63]
Nb steel	0.002–0.1 Nb	1100–1250	2.6–6.2	256–515	[67]
Nb-Ti steel	Base Steel 0.059 Nb 0.062 Nb–0.026 To	850–960 850–1050 1000–1150	4.20 6.75 12.82	34.63 27.45 65.96	[68]
Al-killed plain carbon steel	–	950–1150	3.4	1291	[69]
Medium carbon steel with Al	–	850–950 1000–1100	2.44	53.01 83.42	[70]
V steel	0.28 V	<950 >950	14.7 7.87	115 195	[71]
Ti-Nb steel	0.135 Ti–0.056 Nb	850–1300	2.4	469.36	[72]
Nb steel	0.044 Nb	950–1200	2.5	397.68	[73]

Table 2 Reported values of n and Q for austenitic stainless steels

Material	Special elements (wt%)	Temperature (°C)	n	Q (kJ/mol)	References
304	–	850–1050	6.54–2.16	279.8	[15]
316L	–	850–1050	21.74–3.06	567.9	[15]
316L	–	900–1100	6.25–2.77	–	[82]
High purity 304L	$C<0.0005$	1050	2.25	242	[76]
301LN	0.15 N	800–1000	2.8–2.4	–	[77]
Fe–25Ni–18Cr–3Al	0 Y 0.05 Y	1200–1290	3.85 4.35	299.5 402.2	[78]
Microalloyed 204Cu	0 Nb 0.05 Nb 0.45 Nb	700–1100	3.9–3.1 5.1–3.7 8.1–6.5	363 364 458	[79]
304L	0.15 Mo—0.24 Cu—0.1 V	750–900	5.8–4.8	455	[80]
316LB	100 ppm B	900–1200 1200–1300	–	53.0 318.5	[81]

Mo or microalloying elements and elements, the value of Q is comparable to that of lattice diffusion in austenite (~ 280 kJ/mol [75]) and the value of n generally decreases by increasing temperature towards the ideal value of 2 [76]. For the AISI 301LN austenitic stainless steel, it has been stated that annealing at higher temperatures relieves the residual strains, dissolves the precipitates and increases the atomic migration along the grain boundaries, which promote the loss of grain curvature and texture; all of which lead to a decreased n value [77]. However, for the majority of alloys, the values of n and Q are generally larger, which can be related to the effect of impurities and alloying elements [15]. For instance, for AISI 304 steel, a Q value of 279.8 kJ/mol was obtained while for AISI 316L steel, the value of Q increased to 567.9 kJ/mol due to the strong pinning effect of solute Mo [15]. The similar solute drag effect has been also reported for the yttrium-containing alloys, where by Y addition, the value of Q increased from 299.5 to 402.2 kJ/mol [78]. For an AISI 204Cu steel, the value of Q increased considerably with Nb microalloying from 363 to 458 kJ/mol due to the formation of NbC that creates back-stress on grain boundaries hindering their motion [79]. For an AISI 304L stainless steel microalloyed with V and Mo, the Q value of 455 kJ/mol was determined, which was related to the formation of complex carbonitrides [80]. For an AISI 316LB steel, below and above 1200 °C, the Q values of 53 and 318.5 kJ/mol were obtained, respectively. The Q_v value for volume diffusion of boron in austenite is 87.9 kJ/mol. Based on the general approximation of $Q_{gb}=0.6Q_v$, the value of Q_{gb} of 52.7 kJ/mol can be obtained, which is comparable to the

obtained Q value of 53 kJ/mol for grain growth at temperatures below 1200 °C. This suggests that grain growth in the lower temperature regime occurs by grain boundary diffusion of boron in types 316LB stainless steel [81].

Many studies have done on the Mg alloys as summarized in Table 3, especially on the commercially important AZ31 alloys including 3 wt% Al and 1 wt% Zn. For this alloy, it can be seen that the value of n is ~ 5, indicating the inhibition of grain growth due to the presence of second-phase particles [60]. Moreover, the obtained values of Q are near that for grain boundary diffusion in pure Mg (92 kJ/mol) and for lattice self-diffusion in pure Mg (135 kJ/mol) [83]. The crystallographic texture [84], severe plastic deformation [85], and the presence of solutes and second phase particles [86] have an influence on the obtained values of n and Q. The Gd-containing Mg alloys have shown greater thermal stability compared to the conventional Mg alloys due to the solute segregation to grain boundaries and the presence of intermetallic compounds with high thermal stability [87].

Parameters of the empirical power-law model for aluminum alloys are summarized in Table 4. For ECAP deformed commercially pure (CP) Al, two regimes of grain growth were observed: as temperatures lower than 275 °C, Q value of 49 kJ/mol was obtained while temperatures higher than 300 °C resulted in the Q value of 85 kJ/mol, which is close to the value for grain boundary diffusion in aluminum, 84 kJ/mol. The low Q at low temperatures was related to some changes such as the recovery of the dislocation structures, boundary transforming to equilibrium grain boundary structure, and grain structure becoming coarser and more equiaxed. With increasing annealing temperature, the Q value was found to increase to approach that for grain boundary diffusion in coarse-grained materials, which was attributed to the fact that an equilibrium boundary structure was restored during grain growth [92]. The grain growth kinetics of precipitation-hardening Al-Cu alloys has received considerable attention, where the restriction of grain growth can be verified by the obtained kinetics parameters. However, at high temperatures, the dissolution of phases and elimination of particle-pinning forces enhance the rate of grain growth [93]. In these alloys, different Q values have been obtained: 94.4 kJ/mol [93] close to the value of 84 kJ/mol for grain boundary diffusion in Al and 157.1 kJ/mol [94] close to the value of 142 kJ/mol for volume diffusion in Al [95]. Based on the modeling of the grain growth kinetics by cellular automaton, a high value of 3.94 for n was obtained for grain growth in polycrystalline aluminum at 350 °C following recrystallization. This was related to the anisotropic boundary energy and mobility values, which depend upon misorientation between the crystals [96].

Table 5 summarizes the reported grain growth parameters for Ti alloys. An interesting observation is that the values of n for titanium alloys are low compared to other alloys [97]. For these alloys, there are many reports stating that the value of Q increases with increasing soaking time, which can be primarily explained by the solute drag effect. The velocity of grain boundary migration is faster than the diffusion of solute atoms at the early stage of annealing, leading to lower activation energies. However, due to the increase in the average grain size and the consequent decrease in the grain

Table 3 Reported values of n and Q for magnesium alloys

Material	Condition	Temperature (°C)	n	Q (kJ/mol)	References
AZ31	Rolled	260–450	5	115	[60]
AZ31	Ultrafine grained	350–450	5	105	[83]
AZ31	Hot pressed	300–400	5	110	[88]
AZ31	Hot rolled	250to 450	4	80.8	[84]
Mg-6Zn	Extruded	200–350	4	95.45	[86]
ZG31	Hot rolled	200–500	2.19–2.42	101	[87]
Mg-4.8Gd-1.2Al-1Zn	Extruded	400	5.75	–	[19]
Mg-Sc	Hot rolled	300–450	3	~82	[89]
Mg-9Gd-4Y-0.4Zr	Extruded	400–450	0.04–0.28	147	[90]
Mg-2Gd-1Zn	Extruded	350–450	5.1–4.4	109.6	[91]

Table 4 Reported values of n and Q for aluminum alloys

Material	Condition	Temperature (°C)	n	Q (kJ/mol)	References
AA1050	ECAP processed	< 275 > 300	2 2	49 85	[92]
Al-4.7Cu	–	510–540	2.3–2.5	94.4	[93]
2024	Heat treated	250–350	8.62–8.26	157.1	[94]
Polycrystalline Al	Recrystallized	350	3.94	–	[96]

Table 5 Reported values of n and Q for titanium alloys

Material	Temperature (°C)	Time (min)	Q (kJ/mol)	n	References
Ti–6Al–4V	1000–1260	5–90	227	8.9–3.9	[49]
Ti–4733	850to 1000	30–240	465–895	2.56–5.56	[97]
Ti–5553	850–1000	30–240	187–547	2.56–8.33	[97]
TG6	1055–1075	0.2–180	120.4–212.5	2.63–2.86	[105]
Ti17	905–925	0.2–180	290.5–378.5	3.33–3.70	[105]
Ti–2Al–9.2Mo–2Fe	820–1000	30–720	442.8–644.3	4.63–10.63	[98]
TC4-DT	985–1005	2–120	86.8–129.7	2.86–2.94	[106]
Beta21S	810–960	30–600	320	8–10	[99]
Beta21S-0.1B	810–960	30–600	914	16–53	[99]
Titanium	700–1100	3–120	α: 100 β: 21	1.67–20	[100]
Ti-0.2Pd	700–1100	3–120	α: 133 β: 56	3.33–20	[100]
α-Ti	700–800	5–120	100	2.22–2.33	[101]
β-Ti	900–1100	5–120	20	2–20	[101]
Ti–44Al	1350	2–1200	81	5.88	[107]
Ti–44Al–0.15Gd	1350	2–1200	50	22.2	[107]

boundary area, the driving force of grain growth decreases as the annealing time increases. Moreover, decreasing the migration velocity of grain boundary helps the segregation of solutes at boundaries, which induces the drag effect, and the activation energy for grain growth increases with increasing the solution time [97]. For example, in the case of Ti–2Al–9.2Mo–2Fe, the high content of Mo element (9.2%) with low diffusivity in Ti matrix retards the mobility of grain boundaries more strongly and induces strong drag effects [98]. However, the calculated grain growth parameters for Ti–6Al–4V with a relatively strong initial texture suggested a slow initial grain growth, which was followed by a much quicker growth after the reduction of the texture sharpness at long annealing times [49]. Besides the solute drag effect, the Zener pinning effect also increases the activation energy for grain growth in these alloys [99]. Another important matter that needs to be mentioned is that the Q values considerably differ between the two phases (α and β) in each alloy, which is related to the fact that the α phase has a hexagonal structure and the β phase has a bcc structure. The latter structure is more open and therefore expected to result in a higher growth rate and lower Q values [100]. Therefore, the value of n decreases at temperatures above the β-transus [101]. Moreover, for Ti–15Mo–2.6Nb–3Al–0.2Si alloy, it has been shown that B addition increases the β transus temperature to temperatures higher than 810 °C, which in turn restricts the β grain growth at temperatures near 810 °C as residual α is present in the microstructure [99]. The value of Q is not usually consistent with the lattice self-diffusion activation energy, which can be related to the pinning effects and the fact that the lattice self-diffusion activation energy has been obtained for a nearly pure Ti alloy [102]. The latter effect has been considered for complexly alloyed austenite phases in steels based on the assumption that the activation energy of grain growth is proportional to the activation energy of bulk self-diffusion, which is calculated as a function of the chemical composition of the solid solution [103]. The n value is higher than 2 for most titanium alloys, where the solute drag effect plays a pivotal role in the explanation of this effect [104].

Table 6 summarizes the reported grain growth parameters for high-entropy alloys. The n values greater than two have been reported due to the controlling of grain boundary migration by solute drag effect, the presence of precipitates, and the sluggish nature of diffusion in these alloys [108]. The value of Q is much higher than conventional alloys, which is related to a greater degree of disorder, i.e., a more random state [109]. Since these

Table 6 Reported values of n and Q for high-entropy alloys

Material	Condition	Temperature (°C)	n	Q (kJ/mol)	References
HfNbTaTiZr	Cold rolled	1000–1200	2.2–2.4	303	[14]
FeCoNiCrMn	Cold rolled	900	2.3	420.9	[110]
FeCoNiCrMn	Cold rolled	850–925	3	321.7	[111]
FeCoNiCrMn	Ball milled	800–1100	3.08	197	[112]
Al0.1CoCrFeNi	Cold rolled	950–1150	3	179	[113]
Al0.3CoCrFeNi	Cold rolled	950–1150	3	486	[113]

alloys have several principal elements, it is a hard task to correlate Q with the self-diffusion activation energy of constituents. However, it has been argued that the slowest species control the lattice diffusion rate [14].

On the theoretical front, in the ideal state, grain growth is controlled only by diffusion. In this case, the exponent $n=2$ is used. Furthermore, grain growth can be controlled, for example, by diffusion together with the precipitation phase in growing grains, the exponent $n=3$ is used. If the common effect of precipitation and diffusion along grain boundaries is observed, the exponent $n=4$ is used. In the case when the grain growth is mainly influenced by precipitation, the exponent is close to the value $n=5$ [114].

4 Abnormal grain growth

4.1 Criteria for identification of AGG

Excessive growth of selected grains during AGG may lead to the appearance of grains on the order of millimeters [115]. Since this process shows kinetics similar to primary recrystallization, it is also called secondary recrystallization [116]. A criterion to determine whether a grain in matrix with the mean grain size of $\overline{D}$ is growing abnormally can be written as $d(D_{\text{Abnormal}}/\overline{D})/\mathrm{d}t > 0$, where D_{Abnormal} is the size of the large candidate abnormal grain [117]. A topological criterion can be written as $\mathrm{d}N_A/\mathrm{d}t > 0$, where N_{A} is the number of faces of the abnormal grain. This criterion shows that an abnormal grain grows by gaining faces [118]. It has been also stated that the AGG process is commenced when $D_{\text{Max}}/\overline{D} > 5$ [119] as shown in Fig. 10, where D_{Max} is the size of the coarsest grain [120].

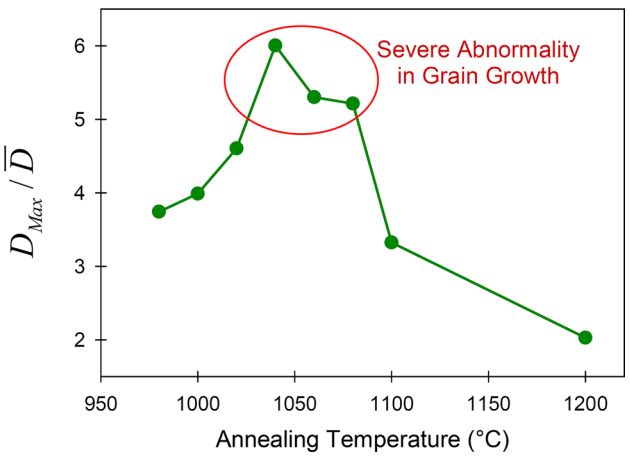

Fig. 10 Ratio of the size of the maximum observed grain to the average size at different temperatures for Hi–B Steel [120]

4.2 Mechanisms and factors lead to AGG

Abnormal growth can take place when some degree of restriction to grain growth in the matrix is present [2]. The second-phase particles, texture, and surface effects are the major factors that lead to AGG [3]. Other factors such as the anisotropy in grain boundary energy, anisotropy in grain boundary mobility, the pre-existence of grains with a size advantage, local fluctuations of grain size/number of particles adjacent to a certain grain, and nature of the interface can contribute to or even provoke the initiation of AGG [121]. However, it has been argued that AGG can be also induced by the solute drag effect in homogeneous systems without any texture, anisotropy of grain boundary mobility and/or energy, pinning particles, and grain size advantage. The solute drag effect can cause AGG under the specific circumstance in which a portion of the grain boundaries in a system break away the solute atmosphere. If such AGG takes place, its kinetics and morphological features will strongly depend on the solute diffusivity, the initial grain size and the interaction strength between solute atoms and grain boundaries. The necessary conditions for the AGG accompanying the grain boundary segregation are as follows: first, a critical driving force must exist where grain boundary velocity jumps discontinuously. Second, only a minor portion of the grain boundaries in the system should break away the segregated solute atom, while the non-segregated atoms drag the other grain boundaries [122].

The effect of particles has been discussed in Sect. 2.2.2, where Fig. 5 shows the effect of particle dispersion level (f/d) on the occurrence of AGG. Based on Fig. 5, if annealing results in the particle coarsening (increase of d) or leads to the decrease of the volume fraction by dissolution (decrease of f), AGG will become more likely if the average grain size does not increase proportionately [3]. This idea has been even successfully utilized for the effect of martensite particles on the occurrence of AGG in DP steels [37]. As a renown example, effective normal grain growth inhibition can be achieved by AlN particles in steels, but their coarsening and dissolution lead to AGG at high temperatures. Conversely, coarse and insoluble inclusions are less effective in preventing normal grain growth of steels, but their stability prevents AGG [4]. Another example is the occurrence of AGG in the extruded Mg–3Gd–3Al–1Zn alloy with the dispersion of Al_2Gd and $(Mg,Al)_3Gd$ phases at 400 C ($\sim 0.75T_{\text{m}}$) [19]. The occurrence of AGG was also observed in DP steel at the intercritical annealing temperature, where after the formation of the equilibrium volume fraction of austenite (or martensite after quenching) in the ferritic matrix, further holding at the intercritical annealing temperature led to the coarsening of these particles during the growth of ferrite grains [16]. In the case of Mg–3Gd–3Al–1Zn alloy (Fig. 11a) [19] and DP steel

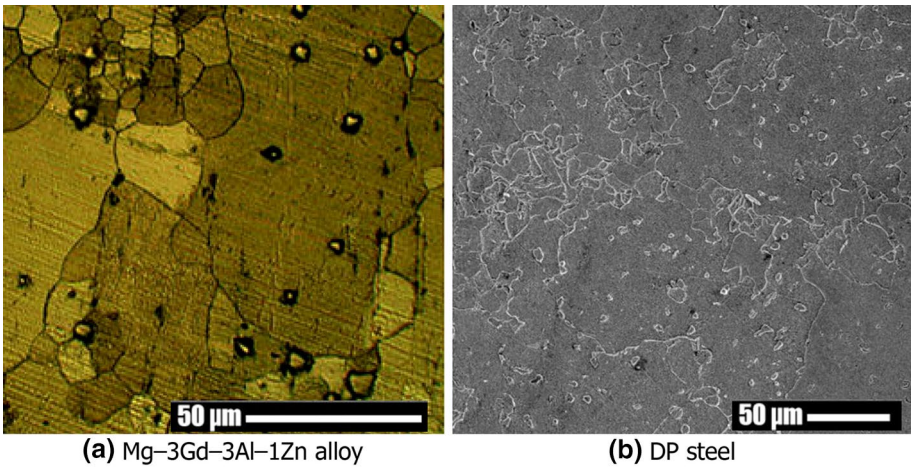

Fig. 11 Remnant particles observed inside abnormally grown grains [18, 19]

(Fig. 11b) [18], the remnant Al_2Gd and martensite particles were observed inside abnormally grown grains, respectively. This might support the argument stating that AGG is caused by disperse particles incapable to move with the boundaries, where the enhancement of the mobility of disperse particles can prevent AGG [116].

A single strong texture component might lead to AGG [123]. During high-temperature annealing of Fe-Si alloys, a few near Goss {110} <001> grains grow exclusively fast and consume the matrix grains, which has a technological importance for magnetic applications [124]. Therefore, the grains which have near Goss orientation have a special advantage over other grains, where the solid-state wetting mechanism has been proposed for it. Based on this mechanism, a grain wets or penetrates the grain boundary or the triple junction of its neighboring grains. This can explain the AGG phenomena such as high growth rate, irregular boundaries, and the formation of numerous peninsular and island grains as shown in Fig. 12 [11]. This mechanism has been recently suggested for AGG in magnesium alloys [19], austenitic stainless steels [6], and DP steels [16]. The occurrence of AGG when precipitates begin to dissolve might indicate that it occurs mainly via triple junction wetting. The precipitates at the triple junction would dissolve faster than those at the other locations due to the faster kinetics of diffusion at the triple junction. This situation would allow the triple junction wetting to occur extensively, whereas grain growth via a non-wetting mode is inhibited by precipitates that have not yet dissolved [11].

Another associated phenomenon for the occurrence of AGG has been also proposed. When Ni was annealed in a carburizing atmosphere, AGG occurred at temperatures below $0.7T_m$, where all or a fraction of the grain boundaries were found to have faceted hill-and-valley structures. Conversely, normal growth occurred above $0.7T_m$, where all grain boundaries were defaceted with smoothly curved shapes [125]. Similarly, during AGG of AISI 316L stainless steel, some grain boundaries were observed to be faceted with hill-and-valley structures, which was attributed to grain boundary movement with boundary steps either produced by two-dimensional nucleation or existing at the junctions with dislocations [126]. When a Ni-based superalloy heat-treated at 1200 °C, AGG occurred and most of the grain boundaries were observed to be faceted; whereas when heat-treated at 1300 °C, normal grain growth occurred, the grain boundaries are defaceted as shown in Fig. 13 [127].

For friction stir processing (FSP), it has been reported that the primary factors leading to AGG are associated with the inhomogeneous deformation pattern during the friction stir process. The fact that certain combinations of tool rotation rate and traverse rate eliminate AGG suggests that

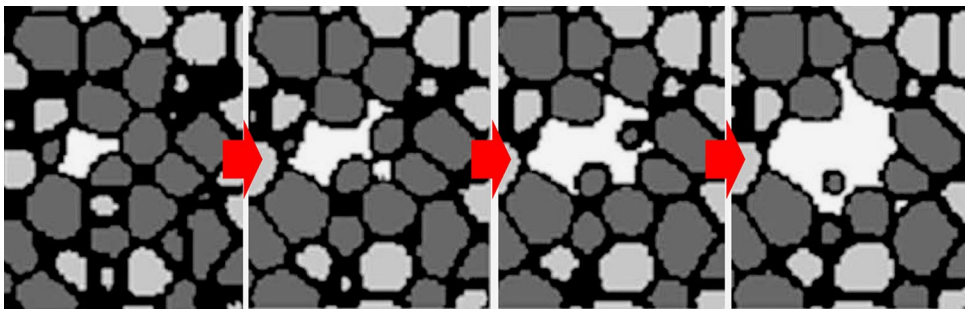

Fig. 12 AGG by solid-state wetting and the formation of peninsular and island grains [11]

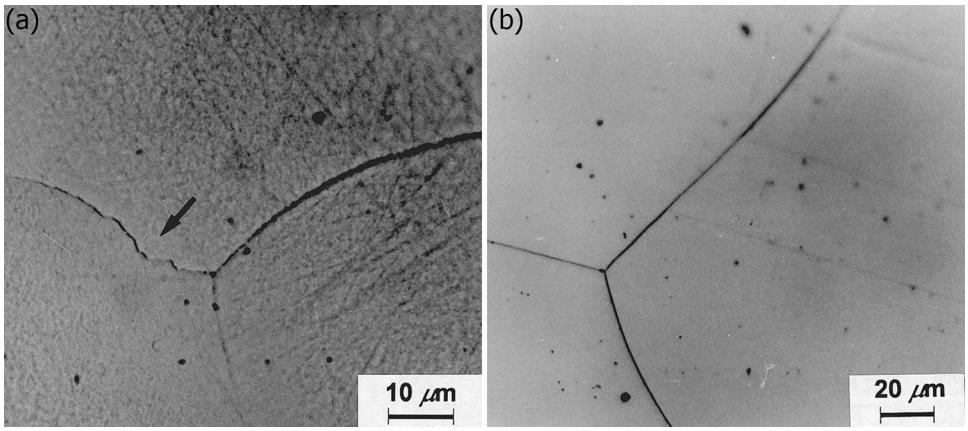

Fig. 13 Typical grain boundaries in a Ni-base superalloy heat-treated for 10 min at **a** 1200 °C (AGG) and **b** 1300 °C (normal growth). The arrow indicates a faceted grain boundary [127]

microstructural uniformity is a key aspect for avoiding AGG [128].

A small plastic strain may prevent normal grain growth [129] and promote the onset of anomalous grain growth [130]. A recent work by Mirzadeh and coworkers [18] revealed that applying a low rolling reduction in thickness before intercritical annealing of DP steels might lead to AGG during intercritical annealing, which can deteriorate the final mechanical properties of the processed sheet [16]. The introduced concept of dynamic abnormal grain growth (DAGG) is also based on the plastic straining for initiation and propagation of AGG [131].

The effects of other factors on AGG have been also studied, which include the cyclic heat treatment [132], solute stabilization of nanocrystalline structure [133], and heating rate during annealing of rapidly solidified alloy [134].

4.3 AGG kinetics

The reported works on the kinetics of abnormal grain growth are discussed in the following. For pure iron [129] and AISI 316L stainless steel [82], it has been shown that the kinetics of AGG can be described by the empirical power law ($D = Kt^{1/n}$), which indicates that the basic assumptions of the grain growth theory are valid. The same cannot be said of normal growth [82]. Grain growth was divided into normal and abnormal growth, and values of the coefficient $1/n$ for both types of growth were determined. The investigations showed that the dependence of $1/n$ on temperature stems from overlapping effects of normal and abnormal grain growth [82].

The progress of AGG may be described by the Johnson–Mehl–Avrami–Kolmogorov (JMAK) kinetics used for recrystallization processes [135]. For instance, the kinetics of AGG in APIX60 steel was investigated [17], where the observed sigmoidal nature of the curve for the fraction of abnormal grains versus time was ascribed to the onset (sometimes referred to as 'nucleation'), growth and impingement of the abnormal grains [136]. The sigmoidal kinetics can be described by the JMAK-type relationship.

It has been also argued that, during AGG, the growth rate of the large/abnormal grains is inversely proportional to the average diameter of the fine grains [17]. In other words, large matrix grains imply slower AGG kinetics, which has been discussed based on the topological theory of abnormal grain growth [137].

5 Future trends

Simulation of grain growth and its validation by experiment, grain growth in nanostructured materials, grain growth in thin films, grain growth during/after solid-state welding processes, grain growth of advanced steels, and grain growth of high-entropy alloys are among the hot topics of recent studies. However, based on its importance, the kinetics of grain growth has remained one of the most widely investigated topics. The present work revealed that while there are similarities in the grain growth kinetics parameters for different engineering alloys, important differences can be also noted. For instance, there is a time dependency of the kinetics parameters in many Ti alloys. These differences are related to the interaction of the material and microstructural factors such as solutes. Therefore, the investigation of the kinetics of grain growth in commercial or newly developed materials via various processing routes constitutes the majority of the future works.

Some of the factors leading to AGG were discussed. The second-phase particles, texture, surface effects, the anisotropy in grain boundary energy, anisotropy in grain boundary mobility, the pre-existence of grains with a size advantage, local fluctuations of grain size/number of particles adjacent to a certain grain, and nature of the interface can contribute to or even provoke the initiation of AGG. It has been even argued that AGG can be also induced by the solute drag effect in homogeneous systems without any texture,

anisotropy of grain boundary mobility and/or energy, pinning particles, and grain size advantage. Therefore, AGG is dependent on many factors, and hence, the processing route and the initial microstructure are important in this regard. Accordingly, understanding the occurrence of AGG in commercial or newly developed materials via various processing routes needs more experimental works.

The proposed mechanisms for AGG such as the solid-state wetting and the grain boundary faceting/defaceting phenomena can explain the observed behavior of many systems. In fact, the occurrence of these mechanisms has been verified for a number of alloy systems in recent works. Therefore, much more experimental/numerical investigations are required to identify the AGG mechanisms and origins. Although being important, the kinetics of AGG remains unraveled and it is expected that this research area receives significant attention.

6 Summary

Recent advances in the kinetics of normal/abnormal grain growth were reviewed in the present work. The following conclusions can be drawn:

1. The effects of temperature, solute drag effect, and Zener pinning on the grain growth kinetics were critically discussed. Moreover, the temperature dependency of the solute drag effect of Mo was clarified in the case of commercial stainless steels. Furthermore, the dissolution of pining particles at elevated temperatures was found to be an important issue, especially in Al and Mg alloy. The grain growth inhibition in duplex alloys was also argued, for which the temperature dependency of phase volume fractions and its effects on the kinetics of grain growth were clarified. Accordingly, the competition of inhibition effect of phase formation and the adverse effect of temperature regarding grain growth resulted in the idea of optimum amount of martensite phase for the maximum inhibition effect in DP steels.
2. The simplifications and the commonly used methods for determination of grain growth exponent (n) and activation energy (Q) in the well-known equations of $D^n - D_0^n = Kt$ and $K = K_0 \exp(-Q/RT)$ were critically discussed. It was proved that the obtained kinetics parameters highly depend on the used method/simplifications. Moreover, it was revealed that the simple equation of $D - D_0 = Kt^{1/n}$ can be alternatively used for studying the kinetics of grain growth without these complications.
3. The obtained values of n and Q for several classes of important engineering alloys such as microalloyed steels, stainless steels, magnesium alloys, aluminum alloys, titanium alloys, and high-entropy alloys (HEAs) were tabulated and discussed. Accordingly, the reasons for the deviation of the kinetics parameters from the theoretically expected values in each system were identified. This includes the presence of impurities and alloying elements, segregation of solutes at boundaries, the presence of second phase particles, strong crystallographic texture, and other factors.
4. The factors leading to AGG such as the coarsening and dissolution of pinning particles and the crystallographic texture were discussed. Moreover, the proposed AGG mechanisms such as the solid-state wetting and the grain boundary faceting/defaceting phenomena were introduced. Furthermore, the kinetics of AGG based on the empirical power law and the similarity of AGG to primary recrystallization in the form of secondary recrystallization were presented. It seems that the subject of AGG needs much more experimental/modeling works to identify its origins and construct suitable models for its kinetics.

Acknowledgements The authors would like to greatly thank the members of the Advanced Steels and Thermomechanically Processed Engineering Materials Laboratory for their help and support. Financial support by the University of Tehran is also gratefully acknowledged.

Funding This work received no funding.

Data availability The authors stated that the processed data required to reproduce these findings were available in this manuscript.

Compliance with ethical standards

Conflict of interest The authors declare no conflict of interest.

Ethical statement The manuscript has been prepared by the contribution of all authors, it is the original authors' work, it has not been published before, it has been solely submitted to this journal, and if accepted, it will not be submitted to any other journal in any language.

References

1. Hillert M. On the theory of normal and abnormal grain growth. Acta Metall. 1965;13:227–38.
2. Rios PR, Zöllner D. Critical assessment 30: grain growth–unresolved issues. Mater Sci Technol. 2018;34:629–38.
3. Humphreys J, Rohrer GS, Rollett A. Recrystallization and related annealing phenomena. 3rd ed. Oxford: Elsevier; 2017.
4. Gladman T. The theory and inhibition of abnormal grain growth in steels. JOM. 1992;44:21–4.
5. Verlinden B, Driver J, Samajdar I, Doherty RD. Thermomechanical processing of metallic materials. Amsterdam: Elsevier; 2007.
6. Shirdel M, Mirzadeh H, Parsa MH. Abnormal grain growth in AISI 304L stainless steel. Mater Charact. 2014;97:11–7.

7. Sun Y, Fujii H. Effect of abnormal grain growth on microstructure and mechanical properties of friction stir welded SPCC steel plates. Mater Sci Eng A. 2017;694:81–92.
8. Simpson CJ, Aust KT, Winegard WC. The four stages of grain growth. Metall Trans. 1971;2:987–91.
9. Miodownik MA. A review of microstructural computer models used to simulate grain growth and recrystallisation in aluminium alloys. J Light Met. 2002;2:125–35.
10. Peng H, Jian Z, Liu F. Review of thermo-kinetic correlation during grain growth in nanocrystalline materials. Int J Ceram Eng Sci. 2020;2:49–65.
11. Ko KJ, Cha PR, Srolovitz D, Hwang NM. Abnormal grain growth induced by sub-boundary-enhanced solid-state wetting: analysis by phase-field model simulations. Acta Mater. 2009;57:838–45.
12. Heidarzadeh A. Tensile behavior, microstructure, and substructure of the friction stir welded 70/30 brass joints: RSM EBSD, and TEM study. Arch Civ Mech Eng. 2019;19:137–46.
13. Chen XM, Lin YC, Wu F. EBSD study of grain growth behavior and annealing twin evolution after full recrystallization in a nickel-based superalloy. J Alloy Compd. 2017;724:198–207.
14. Chen S, Tseng KK, Tong Y, Li W, Tsai CW, Yeh JW, Liaw PK. Grain growth and Hall-Petch relationship in a refractory HfNbTaZrTi high-entropy alloy. J Alloy Compd. 2019;795:19–26.
15. Naghizadeh M, Mirzadeh H. Elucidating the effect of alloying elements on the behavior of austenitic stainless steels at elevated temperatures. Metall Mater Trans A. 2016;47:5698–703.
16. Najafkhani F, Mirzadeh H, Zamani M. Effect of intercritical annealing conditions on grain growth kinetics of dual phase steel. Met Mater Int. 2019;25:1039–46.
17. Zhou TH, Zurob HS. Abnormal and post-abnormal austenite grain growth kinetics in Nb–Ti microalloyed steels. Can Metall Q. 2011;50:389–95.
18. Nikkhah S, Mirzadeh H, Zamani M. Fine tuning the mechanical properties of dual phase steel via thermomechanical processing of cold rolling and intercritical annealing. Mater Chem Phys. 2019;230:1–8.
19. Pourbahari B, Mirzadeh H, Emamy M. Elucidating the effect of intermetallic compounds on the behavior of Mg–Gd–Al–Zn magnesium alloys at elevated temperatures. J Mater Res. 2017;32:4186–95.
20. Gottstein G, Shvindlerman LS. Grain boundary migration in metals: thermodynamics, kinetics, applications. 2nd ed. Boca Raton: CRC; 2010.
21. Chamanfar A, Chentouf SM, Jahazi M, Lapierre-Boire LP. Austenite grain growth and hot deformation behavior in a medium carbon low alloy steel. J Mater Res Technol. 2020;9:12102–14.
22. Xu Y, Liu J, Zhao Y, Jiao Y. Austenite grain growth kinetics and mechanism of grain growth in 12Cr ultra-super-critical rotor steel. Philos Mag. 2021;101:77–95.
23. Kheiri S, Mirzadeh H, Naghizadeh M. Tailoring the microstructure and mechanical properties of AISI 316L austenitic stainless steel via cold rolling and reversion annealing. Mater Sci Eng A. 2019;759:90–6.
24. Naghizadeh M, Mirzadeh H. Microstructural evolutions during reversion annealing of cold-rolled AISI 316 austenitic stainless steel. Metall Mater Trans A. 2018;49:2248–56.
25. Sohrabi MJ, Mirzadeh H, Dehghanian C. Significance of martensite reversion and austenite stability on the mechanical properties and TRIP effect of austenitic stainless steels. J Mater Eng Perform. 2020;29:3233–42.
26. Krauss G. Steels processing, structure, and performance. 2nd ed. Materials Park: ASM International; 2015.
27. Gómez M, Medina SF. Role of microalloying elements in the microstructure of hot rolled steels. Int J Mater Res. 2011;102:1197–207.
28. Bayat-Tork N, Mahmudi R, Hoseini-Athar MM. Hot deformation constitutive analysis and processing maps of extruded Mg–Gd binary alloys. J Mater Res Technol. 2020;9:15346–59.
29. Lin YC, Wu XY, Chen XM, Chen J, Wen DX, Zhang JL, Li LT. EBSD study of a hot deformed nickel-based superalloy. J Alloy Compd. 2015;640:101–13.
30. Garcia-Bernal MA, Mishra RS, Verma R, Hernández-Silva D. Inhibition of abnormal grain growth during hot deformation behavior of friction stir processed 5083 Al alloys. Mater Sci Eng A. 2015;636:326–30.
31. Abbaschian R, Abbaschian L, Reed-Hill RE. Physical metallurgy principles. 4th ed. Boston: Cengage Learning; 2009.
32. Suryanarayana C, Koch CC. Nanocrystalline materials—current research and future directions. Hyperfine Interact. 2000;130:5–44.
33. Fu LM, Wang HR, Wang W, Shan AD. Austenite grain growth prediction coupling with drag and pinning effects in low carbon Nb microalloyed steels. Mater Sci Technol. 2011;27:996–1001.
34. Suikkanen P, Karjalainen P, DeArdo AJ (2009) Effect of carbon content on the phase transformation characteristics, microstructure and properties of 500 MPa grade microalloyed steels with nonpolygonal ferrite microstructures, la metallurgia italiana 41–54
35. Staśko R, Adrian H, Adrian A. Effect of nitrogen and vanadium on austenite grain growth kinetics of a low alloy steel. Mater Char. 2006;56:340–7.
36. Humphreys FJ. A unified theory of recovery, recrystallization and grain growth, based on the stability and growth of cellular microstructures—II The effect of second-phase particles. Acta Mater. 1997;45:5031–9.
37. Jamei F, Mirzadeh H, Zamani M. Synergistic effects of holding time at intercritical annealing temperature and initial microstructure on the mechanical properties of dual phase steel. Mater Sci Eng A. 2019;750:125–31.
38. Graux A, Cazottes S, De Castro D, San Martín D, Capdevila C, Cabrera JM, Molas S, Schreiber S, Mirkovic D, Danoix F, Bugnet M, Fabregue D, Perez M. Precipitation and grain growth modelling in Ti–Nb microalloyed steels. Materialia. 2019;5:100233.
39. Grajcar A, Borek W. Thermo-mechanical processing of high-manganese austenitic TWIP-type steels. Arch Civ Mech Eng. 2008;8:29–38.
40. Maalekian M, Radis R, Militzer M, Moreau A, Poole WJ. In situ measurement and modelling of austenite grain growth in a Ti/Nb microalloyed steel. Acta Mater. 2012;60:1015–26.
41. Giuliano G. Superplastic forming of advanced metallic materials. Sawton: Woodhead Publishing; 2011.
42. Langdon TG. Seventy-five years of superplasticity: historic developments and new opportunities. J Mater Sci. 2009;44:5998–6010.
43. Lin YC, Xiao YW, Jiang YQ, Pang GD, Li HB, Zhang XY, Zhou KC. Spheroidization and dynamic recrystallization mechanisms of Ti-55511 alloy with bimodal microstructures during hot compression in $\alpha+\beta$ region. Mater Sci Eng A. 2020;782:139282.
44. Chen MS, Zou ZH, Lin YC, Li HB, Wang GQ. Formation mechanism of large grains inside annealed microstructure of GH4169 superalloy by cellular automation method. J Mater Sci Technol. 2019;35:1403–11.
45. Chen MS, Zou ZH, Lin YC, Li HB, Wang GQ, Ma YY. Microstructural evolution and grain refinement mechanisms of a Ni-based superalloy during a two-stage annealing treatment. Mater Char. 2019;151:445–56.
46. Takayama T, Wey M, Nishizawa T. Grain growth in dual-phase steel. Tetsu-to-Hagané. 1982;68:1016–23.
47. Azeem MA, Tewari A, Ramamurty U. Effect of recrystallization and grain growth on the mechanical properties of an extruded AZ21 Mg alloy. Mater Sci Eng, A. 2010;527:898–903.

48. Ralph B. Grain growth. Mater Sci Technol. 1990;6:1136–44.
49. Ivasishin OM, Shevchenko SV, Semiatin SL. Effect of crystallographic texture on the isothermal beta grain-growth kinetics of Ti–6Al–4V. Mater Sci Eng A. 2002;332:343–50.
50. Pourbahari B, Mirzadeh H, Emamy M, Roumina R. Enhanced ductility of a fine-grained Mg–Gd–Al–Zn magnesium alloy by hot extrusion. Adv Eng Mater. 2018;20:1701171.
51. Beck PA, Holzworth ML, Hu H. Instantaneous rates of grain growth. Phys Rev. 1948;73:526–7.
52. Burke JE, Turnbull D. Recrystallization and grain growth. Progress Metal Phys. 1952;3:220–92.
53. Sellars CM, Whiteman JA. Recrystallization and grain growth in hot rolling. Metal Sci. 1979;13:187–94.
54. Nishizawa T. Grain growth in single-and dual-phase steels. Tetsu-to-hagané. 1984;70:194–202.
55. Dong D, Chen F, Cui Z. Modeling of austenite grain growth during austenitization in a low alloy steel. J Mater Eng Perform. 2016;25:152–64.
56. Raghunathan N, Sheppard T. Microstructural development during annealing of hot rolled Al–Mg alloys. Mater Sci Technol. 1989;5:542–7.
57. Anelli E. Application of mathematical modelling to hot rolling and controlled cooling of wire rods and bars. ISIJ Int. 1992;32:440–9.
58. Du S, Li Y, Zheng Y. Kinetics of austenite grain growth during heating and its influence on hot deformation of LZ50 steel. J Mater Eng Perform. 2016;25:2661–9.
59. Xu Y, Tang D, Song Y, Pan X. Prediction model for the austenite grain growth in a hot rolled dual phase steel. Mater Des. 2012;36:275–8.
60. Bhattacharyya JJ, Agnew SR, Muralidharan G. Texture enhancement during grain growth of magnesium alloy AZ31B. Acta Mater. 2015;86:80–94.
61. Park JH, Tomota Y, Wey MY. Suppression of grain growth in dual phase steels. Mater Sci Technol. 2002;18:1517–23.
62. Illescas S, Fernández J, Guilemany JM. Kinetic analysis of the austenitic grain growth in HSLA steel with a low carbon content. Mater Lett. 2008;62:3478–80.
63. Azizi G, Mirzadeh H, Parsa MH. Unraveling the effect of homogenization treatment on decomposition of austenite and mechanical properties of low-alloyed TRIP steel. Steel Res Int. 2016;87:820–3.
64. Simpson CJ, Aust KT, Winegard WC. Activation energies for normal grain growth in lead and cadmium base alloy. Metall Trans. 1971;2:993–7.
65. Pawlak K, Białobrzeska B, Konat Ł. The influence of austenitizing temperature on prior austenite grain size and resistance to abrasion wear of selected low-alloy boron steel. Arch Civ Mech Eng. 2016;16:913–26.
66. Yue C, Zhang L, Liao S, Gao H. Kinetic analysis of the austenite grain growth in GCr15 steel. J Mater Eng Perform. 2010;19:112–5.
67. Annan KA, Siyasiya CW, Stumpf WE. Austenite grain growth kinetics after isothermal deformation in microalloyed steels with varying Nb concentrations. ISIJ Int. 2018;58:333–9.
68. An X, Tian Y, Wang H, Shen Y, Wang Z. Suppression of austenite grain coarsening by using Nb–Ti microalloying in high temperature carburizing of a gear steel. Adv Eng Mater. 2019;21:1900132.
69. Militzer M, Giumelli A, Hawbolt EB, Meadowcroft TR. Austenite grain growth kinetics in Al-killed plain carbon steels. Metall Mater Trans A. 1996;27:3399–409.
70. Liu Z, Bao Y, Wang M, Li X, Zeng F. Austenite grain growth of medium-carbon alloy steel with aluminum additions during heating process. Int J Miner Metall Mater. 2019;26:282–90.
71. Yang G, Sun X, Yong Q, Li Z, Li X. Austenite grain refinement and isothermal growth behavior in a low carbon vanadium microalloyed steel. J Iron Steel Res Int. 2014;21:757–64.
72. Yang HL, Xu G, Wang L, Yuan Q, He B. A study of growth of austenite grains in a steel microalloyed with Ti and Nb. Met Sci Heat Treat. 2017;59:8–13.
73. Zhao Y, Shi J, Cao W, Wang M, Xie G. Kinetics of austenite grain growth in medium-carbon niobium-bearing steel. J Zhejiang Univ Sci A. 2011;12:171–6.
74. Di Schino A, Kenny JM, Abbruzzese G. Analysis of the recrystallization and grain growth processes in AISI 316 stainless steel. J Mater Sci. 2002;37:5291–8.
75. Mirzadeh H, Cabrera JM, Najafizadeh A. Constitutive relationships for hot deformation of austenite. Acta Mater. 2011;59:6441–8.
76. Gavard L, Montheillet F, Le Coze J. Recrystallization and grain growth in high purity austenitic stainless steels. Scripta Mater. 1998;39:1095–9.
77. Rajasekhara S, Ferreira PJ. Martensite→ austenite phase transformation kinetics in an ultrafine-grained metastable austenitic stainless steel. Acta Mater. 2011;59:738–48.
78. Zhao WX, Wu Y, Jiang SH, Wang H, Liu XJ, Lu ZP. Microalloying effects of yttrium on recrystallization behavior of an alumina-forming austenitic stainless steel. J Iron Steel Res Int. 2016;23:553–8.
79. Kisko A, Talonen J, Porter DA, Karjalainen LP. Effect of Nb microalloying on reversion and grain growth in a high-Mn 204Cu austenitic stainless steel. ISIJ Int. 2015;55:2217–24.
80. Sabooni S, Karimzadeh F, Enayati MH. Thermal stability study of ultrafine grained 304L stainless steel produced by martensitic process. J Mater Eng Perform. 2014;23:1665–72.
81. Kashyap BP, Tangri K. Grain growth behaviour of type 316L stainless steel. Mater Sci Eng, A. 1992;149:L13–6.
82. Mizera J, Wyrzykowski JW, Kurzydłowski KJ. Description of the kinetics of normal and abnormal grain growth in austenitic stainless steel. Mater Sci Eng A. 1988;104:157–62.
83. Ma J, Yang X, Huo Q, Sun H, Qin J, Wang J. Mechanical properties and grain growth kinetics in magnesium alloy after accumulative compression bonding. Mater Des. 2013;47:505–9.
84. Miao Q, Hu L, Wang X, Wang E. Grain growth kinetics of a fine-grained AZ31 magnesium alloy produced by hot rolling. J Alloy Compd. 2010;493:87–90.
85. Young JP, Askari H, Hovanski Y, Heiden MJ, Field DP. Thermal microstructural stability of AZ31 magnesium after severe plastic deformation. Mater Char. 2015;101:9–19.
86. Jin Z, Yu D, Wu X, Yin K, Yan K. Drag effects of solute and second phase distributions on the grain growth kinetics of pre-extruded Mg-6Zn alloy. J Mater Sci Technol. 2016;32:1260–6.
87. Roostaei M, Shirdel M, Parsa MH, Mahmudi R, Mirzadeh H. Microstructural evolution and grain growth kinetics of GZ31 magnesium alloy. Mater Char. 2016;118:584–92.
88. Wang X, Hu L, Liu K, Zhang Y. Grain growth kinetics of bulk AZ31 magnesium alloy by hot pressing. J Alloy Compd. 2012;527:193–6.
89. Silva CJ, Kula A, Mishra RK, Niewczas M. Grain growth kinetics and annealed texture characteristics of Mg-Sc binary alloys. J Alloy Compd. 2016;687:548–61.
90. Alizadeh R, Mahmudi R, Ngan AHW, Langdon TG. Microstructural stability and grain growth kinetics in an extruded fine-grained Mg–Gd–Y–Zr alloy. J Mater Sci. 2015;50:4940–51.
91. Hoseini-Athar MM, Mahmudi R, Babu RP, Hedström P. Effect of Zn content on the microstructural stability and grain growth kinetics of fine-grained extruded Mg–Gd–Zn alloys. J Alloy Compd. 2020;831:154766.

92. Yu CY, Sun PL, Kao PW, Chang CP. Evolution of microstructure during annealing of a severely deformed aluminum. Mater Sci Eng A. 2004;366:310–7.
93. Wierszyłowski I, Stankowiak A, Wieczorek S, Samolczyk J. Kinetics of transformation during supersaturation and aging of the Al-4.7 mass% Cu alloy: grain size, dilatometric, and differential thermal analysis studies. J Phase Equilibr Diffus. 2005;26:555–60.
94. Huda Z, Tuan Z. Kinetics of grain growth in 2024–T3: an aerospace aluminum alloy. J Alloy Compd. 2009;478:128–32.
95. Mirzadeh H. Quantification of the strengthening effect of reinforcements during hot deformation of aluminum-based composites. Mater Des. 2015;65:80–2.
96. Raghavan S, Satyam SS. Modeling the grain growth kinetics by cellular automaton. Mater Sci Eng A. 2007;445:203–9.
97. Sadeghpour S, Javaheri V, Abbasi SM, Kömi J. The effect of phase stability on the grain growth behavior of beta titanium alloys. Phys B. 2020;593:412315.
98. Lee DG, Li C, Lee Y, Mi X, Ye W. Effect of temperature on grain growth kinetics of high strength Ti–2Al–9.2 Mo–2Fe alloy. Thermochim Acta. 2014;586:66–71.
99. Cherukuri B, Srinivasan R, Tamirisakandala S, Miracle DB. The influence of trace boron addition on grain growth kinetics of the beta phase in the beta titanium alloy Ti–15Mo–2.6 Nb–3Al–0.2 Si. Scripta Mater. 2009;60:496–9.
100. Gil FJ, Picas JA, Manero JM, Forn A, Planell JA. Effect of the addition of palladium on grain growth kinetics of pure titanium. J Alloy Compd. 1997;260:147–52.
101. Gil FJ, Planell JA. Behaviour of normal grain growth kinetics in single phase titanium and titanium alloys. Mater Sci Eng A. 2000;283:17–24.
102. Hoseini M, Pourian MH, Bridier F, Vali H, Szpunar JA, Bocher P. Thermal stability and annealing behaviour of ultrafine grained commercially pure titanium. Mater Sci Eng A. 2012;532:58–63.
103. Vasilyev AA, Sokolov SF, Sokolov DF, Kolbasnikov NG. Modeling of grain growth kinetics in complexly alloyed austenite. Lett Mater. 2019;9:419–23.
104. Xu YF, Yi DQ, Liu HQ, Wang B, Yang FL. Age-hardening behavior, microstructural evolution and grain growth kinetics of isothermal ω phase of Ti–Nb–Ta–Zr–Fe alloy for biomedical applications. Mater Sci Eng A. 2011;529:326–34.
105. Wang T, Guo H, Tan L, Yao Z, Zhao Y, Liu P. Beta grain growth behaviour of TG6 and Ti17 titanium alloys. Mater Sci Eng A. 2011;528:6375–80.
106. Peng X, Guo H, Qin C, Shi Z, Zhao Z. Isothermal beta grain growth kinetics of TC4-DT titanium alloy under two different prior processing conditions: deformed vs undeformed. Rare Metal Mater Eng. 2014;43:1855–61.
107. Li W, Xia K. Kinetics of the α grain growth in a binary Ti–44Al alloy and a ternary Ti–44Al–0.15 Gd alloy. Mater Sci Eng A. 2002;329:430–4.
108. Klimova MV, Shaysultanov DG, Zherebtsov SV, Stepanov ND. Effect of second phase particles on mechanical properties and grain growth in a CoCrFeMnNi high entropy alloy. Mater Sci Eng A. 2019;748:228–35.
109. Seol JB, Wung Bae J, Li Z, Chan Han J, Gi Kim J, Raabe D, Seop Kim H. Boron doped ultrastrong and ductile high-entropy alloys. Acta Mater. 2018;151:366–76.
110. Huang YC, Su CH, Wu SK, Lin C. A study on the Hall-Petch relationship and grain growth kinetics in FCC-structured high/medium entropy alloys. Entropy. 2019;21:297.
111. Liu WH, Wu Y, He JY, Nieh TG, Lu ZP. Grain growth and the Hall–Petch relationship in a high-entropy FeCrNiCoMn alloy. Scripta Mater. 2013;68:526–9.
112. Vaidya M, Anupam A, Vijay Bharadwaj J, Srivastava C, Murty BS. Grain growth kinetics in CoCrFeNi and CoCrFeMnNi high entropy alloys processed by spark plasma sintering. J Alloys Compd. 2019;791:1114–21.
113. Gwalani B, Salloom R, Alam T, Valentin SG, Zhou X, Thompson G, Srinivasan SG, Banerjee R. Composition-dependent apparent activation-energy and sluggish grain-growth in high entropy alloys. Mater Res Lett. 2019;7:267–74.
114. Napoli G, Di Schino A. Modelling grain growth kinetics in steels. Arch Metall Mater. 2018;63:839–44.
115. Shirdel M, Mirzadeh H, Parsa MH. Microstructural evolution during normal/abnormal grain growth in austenitic stainless steel. Metall Mater Trans A. 2014;45:5185–93.
116. Novikov VY. Abnormal grain growth: effect of disperse particles. Met Sci Heat Treat. 2018;60:135–41.
117. Rios PR. Some theoretical considerations on abnormal grain growth. Mater Sci Forum. 1996;204:247–56.
118. Zöllner D, Rios PR. Topological changes in coarsening networks. Acta Mater. 2017;130:147–54.
119. Novikov VY. Microstructure evolution during grain growth in materials with disperse particles. Mater Lett. 2012;68:413–5.
120. Su C, Zhao G, Xiao H, Lan Y, Huang F. Abnormal grain growth of hi–b steel in the secondary recrystallization. Metall Microstruct Anal. 2018;7:608–17.
121. Rios PR. Abnormal grain growth in materials containing particles. Acta Metall Mater. 1994;42:839–43.
122. Kim SG, Park YB. Grain boundary segregation, solute drag and abnormal grain growth. Acta Mater. 2008;56:3739–53.
123. Engler O, Huh MY. Evolution of the cube texture in high purity aluminum capacitor foils by continuous recrystallization and subsequent grain growth. Mater Sci Eng A. 1999;271:371–81.
124. Birosca S, Nadoum A, Hawezy D, Robinson F, Kockelmann W. Mechanistic approach of Goss abnormal grain growth in electrical steel: Theory and argument. Acta Mater. 2020;185:370–81.
125. Lee SB, Yoon DY, Hwang NM, Henry MF. Grain boundary faceting and abnormal grain growth in nickel. Metall Mater Trans A. 2000;31:985–94.
126. Choi JS, Yoon DY. The temperature dependence of abnormal grain growth and grain boundary faceting in 316L stainless steel. ISIJ Int. 2001;41:478–83.
127. Lee SB, Yoon DY, Henry MF. Abnormal grain growth and grain boundary faceting in a model Ni-base superalloy. Acta Mater. 2000;48:3071–80.
128. Charit I, Mishra RS. Abnormal grain growth in friction stir processed alloys. Scripta Mater. 2008;58:367–71.
129. Riontino G, Antonione C, Battezzati L, Marino F, Tabasso MC. Kinetics of abnormal grain growth in pure iron. J Mater Sci. 1979;14:86–90.
130. Antonione C, Marino F, Riontino G, Tabasso MC. Effect of slight deformations on grain growth in iron. J Mater Sci. 1977;12:747–50.
131. Ciulik J, Taleff EM. Dynamic abnormal grain growth: a new method to produce single crystals. Scripta Mater. 2009;61:895–8.
132. Omori T, Kusama T, Kawata S, Ohnuma I, Sutou Y, Araki Y, Ishida K, Kainuma R. Abnormal grain growth induced by cyclic heat treatment. Science. 2013;341:1500–2.
133. Donaldson OK, Hattar K, Kaub T, Thompson GB, Trelewicz JR. Solute stabilization of nanocrystalline tungsten against abnormal grain growth. J Mater Res. 2018;33:68–80.
134. Baricco M, Mastrandrea E, Antonione C, Viala B, Degauque J, Ferrara E, Fiorillo F. Grain growth and texture in rapidly solidified Fe (Si) 6.5 wt.% ribbons. Mater Sci Eng A. 1997;226:1025–9.
135. Nasiri Z, Ghaemifar S, Naghizadeh M, Mirzadeh H. Thermal mechanisms of grain refinement in steels: a review. Metals Mater Int. 2020. https://doi.org/10.1007/s12540-020-00700-1.

136. Dunn CG, Walter JL. Secondary recrystallization. In: Margolin H, editor. Recrystallization, grain growth and textures. Metals Park: ASM; 1966. p. 461–521.
137. Rios PR, Glicksman ME. Topological theory of abnormal grain growth. Acta Mater. 2006;54:5313–21.